Experience and new prospects of PET imaging for ion beam therapy monitoring

Katia Parodi [a,*], **Taiga Yamaya** [b], **Pawel Moskal** [c,d]

[a] Ludwig-Maximilians-Universität München, Lehrstuhl für Experimental Physik – Medizinische Physik, Garching b. München, Germany
[b] National Institutes for Quantum Science and Technology, Chiba, Japan
[c] M. Smoluchowski Institute of Physics, Jagiellonian University, Krakow, Poland
[d] Center for Theranostics, Jagiellonian University, Krakow, Poland

Received 26 June 2022; accepted 2 November 2022

Abstract

Pioneering investigations on the usage of positron-emission-tomography (PET) for the monitoring of ion beam therapy with light (protons, helium) and heavier (stable and radioactive neon, carbon and oxygen) ions started shortly after the first realization of planar and tomographic imaging systems, which were able to visualize the annihilation of positrons resulting from irradiation induced or implanted positron emitting nuclei. And while the first clinical experience was challenged by the utilization of instrumentation directly adapted from nuclear medicine applications, new detectors optimized for this unconventional application of PET imaging are currently entering the phase of (pre)clinical testing for more reliable monitoring of treatment delivery during irradiation. Moreover, recent advances in detector technologies and beam production open several new exciting opportunities which will not only improve the performance of PET imaging under the challenging conditions of in-beam applications in ion beam therapy, but will also likely expand its field of application. In particular, the combination of PET and Compton imaging can enable the most efficient utilization of all possible radiative emissions for both stable and radioactive ion beams, while positronium lifetime imaging may enable probing new features of the underlying tumour and normal tissue environment. Thereby, PET imaging will not only provide means for volumetric reconstruction of the delivered treatment and in-vivo verification of the beam range, but can also shed new insights for biological optimization of the treatment or treatment response assessment.

Keywords: Positron emission tomography; Ion beam therapy; Range verification; Positronium imaging

1 Introduction

Ion beam therapy is a still rapidly emerging form of external beam radiotherapy which exploits the advantageous interaction properties of swift ions in matter, especially their finite range and the characteristic dose maximum in depth called Bragg peak [1]. In particular, ion beams can offer steeper dose gradients to enable conformal tumour coverage with better sparing of surrounding normal tissues in comparison to the widely established photon radiation. Moreover, heavier ions like carbon can offer additional biological advantages due to the selective increase of ionization density toward their end of range, providing a differential increase of relative biological effectiveness which can thus enhance the tumor cell killing at the same level of deposited physical dose in the tumour, while still preserving the sparing of the surrounding normal tissue [2]. However, full exploitation of these physical and biological advantages in clinical practice requires a detailed knowledge of the beam stopping position in the patient. To this end, the typical treatment planning approach relies on the semi-empirical calibration of X-ray computed tomography (CT) images of the patient

* Corresponding author: Katia Parodi, Ludwig-Maximilians-Universität München, Lehrstuhl für Experimental Physik – Medizinische Physik, Garching b. München.
E-mail: Katia.Parodi@lmu.de (K. Parodi).

Z Med Phys **33** (2023) 22–34
https://doi.org/10.1016/j.zemedi.2022.11.001
www.elsevier.com/locate/zemedi

into values of stopping power ratios (SPR) of tissue relative to water, in order to translate the experimentally known Bragg position in water to the arbitrary patient anatomy. However, this approach can introduce intrinsic range uncertainties up to ~3% [3], in addition to unavoidable uncertainties in the knowledge of the daily patient anatomy and positioning setup. All these uncertainties result in the conservative introduction of safety margins around the identified clinical target volume, and the avoidance of certain treatment angles stopping the beam just in front of radiosensitive critical organs. Hence, reduction of range uncertainties at the stage of planning or treatment delivery remains a very active field of research in the particle therapy community, where positron emission tomography represents one of the most widely investigated imaging techniques.

Already since the pioneering investigations of ion beam therapy in Berkeley, it was recognized that the at that time just emerging imaging modalities aiming to reconstruct positron emitter distributions from the coincident detection of opposed annihilation gamma rays could provide in-vivo and non-invasive information on the beam stopping position. In fact, as long as the beam energy is above the threshold for nuclear interaction between the incoming beam and the tissue nuclei, positron emitters can be produced and the back-to-back 511 keV photons ensuing from the annihilation of the positron emitted in the radioactive decay can be detected. However, the correlation between the spatial distributions of the annihilation photons origin (in first approximation attributed to the location of the formed positron emitters) and the delivered dose differs depending on the primary ion species and mechanisms behind positron emitter formation (or localization, in case of primary radioactive beams). In particular, incoming stable beams with charge $Z < 5$ can produce positron emitter target fragments (e.g., ^{11}C, ^{15}O) almost all along the primary beam penetration depth, with a pronounced fall-off just shortly before the Bragg peak, depending on the residual range (typically a few millimeters) below the tissue-dependent nuclear reaction thresholds (Fig. 1, left). For ions heavier than protons, this fall-off of the irradiation induced activation is followed by a small tail of activation ascribed to the minor amount of target fragments generated by longer-ranging projectile fragments of the primary beam (Fig. 1, middle). For ions heavier than Beryllium, projectile fragmentation can also result in positron emitting projectile fragments, which generate a more localized activity signal (depending on their stopping position) superimposed onto the pedestal of β^+-emitting target fragments (Fig. 1, right). Especially the isotopic components of the primary stable beam (e.g., ^{11}C from ^{12}C ions) will stop shortly before the Bragg peak, providing a better correlation between the depth distributions of activity and dose for range monitoring in comparison to the case of target fragmentation only [7]. This however typically comes at the expense of a lower amount of activity produced for the same level of therapeutic dose [5], which can challenge the image reconstruction especially in the usual case of a relatively broad irradiation-induced activity distribution compared to localized accumulation of nuclear medicine radiotracers. Hence, an alternative already investigated in the early days of light ion beam therapy and regaining interest now that more powerful accelerator systems are being developed is the implantation of radioactive ion beams [8], which can provide a stronger and localized activity signal almost corresponding to the Bragg peak position [9]. Moreover, the new possibilities opened by advances in detector technologies and data processing can enable the exploitation of additional signatures beyond the annihilation photons, like triple coincidence imaging in the case of β^+-decays accompanied by an additional prompt gamma emission (e.g., ^{10}C and ^{14}O) [10,11], or visualization of the positronium mean lifetime [12–15]. All these new approaches still under investigations can expand the field of application of PET monitoring beyond the scope of range verification, opening new prospects related to biological image guidance and treatment response assessment in the era of personalized medicine, as reviewed in this contribution.

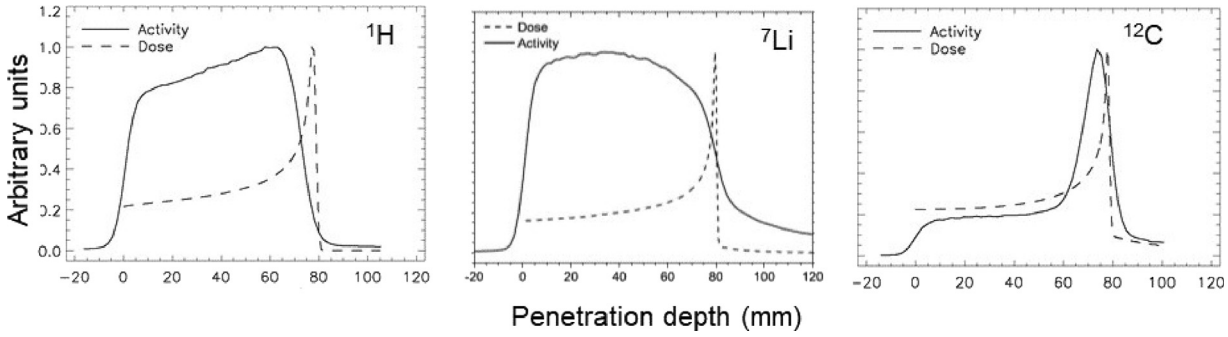

Figure 1. Depth distributions of calculated dose (dashed line) and measured β+-activity (solid line) for ^{1}H (left), ^{7}Li (middle), and ^{12}C (right) ions impinging in homogeneous targets of polymethyl methacrylate (PMMA, $C_5H_8O_2$). (Adapted from references [4,5,6]).

2 Lessons learnt from the first clinical experience of PET monitoring of ion beam therapy

Attempts to exploit both, the irradiation induced activation originated by nuclear interactions of primary stable ions in tissue as well as the localized signal from the stopping position of implanted radioactive ion beams, date back to the early days of particle therapy [8,16,17]. The initial approaches mostly performed in phantoms or animals were relying on dual-head planar cameras which were at that time just at their infancy. And although these studies suffered from several limitations of the used imaging systems, including limited detection efficiency, low to moderate spatial resolution and sensitivity to background radiation for in-beam operation, they indicated the potential of the method to monitor the ion beam range with millimeter accuracy at typical therapeutic doses [8], and even envisioned the potential to aid reconstruction of the delivered dose or support studies of regional blood flow following activation in-vivo [18].

This motivated the efforts toward the first extensive clinical application with a tomographic limited angle dual-head PET scanner pursued within the pilot carbon ion therapy project at GSI Darmstadt. The customized system employed 64 commercial scintillator block detectors of the ECAT EXACT PET scanner (CTI PET Systems Inc., Knoxville, TN), consisting of bismuth germanate (BGO) crystal arrays read out by photomultiplier tubes. The blocks were arranged to cover two spheroid segments of 4×8 detectors each, resulting in a ∼9% solid angle coverage [19]. A customized list mode data acquisition system was developed to enable "in-beam" acquisition during the dose delivery, exploiting the pauses of the pulsed structure from the synchrotron accelerator [19]. The final activity distributions from measured and simulated data were obtained using iterative reconstruction within a few hours after completion of a treatment fraction, thus enabling assessment of the delivery prior to the next fraction for a possible adaptation. The experience in the in-beam PET monitoring of over 440 patients mainly treated for skull base tumours with carbon ions indicated the potential of the method to detect possible delivery errors due to anatomical changes, patient setup errors or incorrect calibration of the planning CT data into SPR values [20]. In particular, it could be shown that even range differences below the moderate spatial resolution (∼5 mm FWHM) of the system could be resolved for data of sufficient signal-to-noise ratio. Also promising attempts for dose quantification could be reported, based on a trial and error approach which applied positional and anatomical changes until the simulated positron emitter distributions could best reproduce the actual PET measurements [20]. The pioneering clinical study however also indicated the challenges of the limited angle system relying on components of a commercial nuclear medicine PET scanner, especially in terms of sensitivity and severe limited angle artifacts, most pronounced for large tumour volumes in extra-cranial anatomical locations (e.g., in the pelvic area) [21].

Further, largely in-silico studies suggested the advantages of in-beam implementations to minimize effects of biological washout processes, loss of activation in the time elapsed between irradiation and imaging, along with possible co-registration issues in case of patient repositioning [22,23]. Nevertheless, most of the subsequent clinical investigations still relied on in-room or offline (i.e., in a different room) implementations based on commercial PET(/CT) scanners originated for nuclear medicine applications, due to their broader availability and issues of in-beam acquisition at continuous wave cyclotrons [24]. A more comprehensive review of the reported clinical applications, mostly limited to small cohorts of patients, can be found in [25]. And although most of these predominantly offline studies with protons and ^{12}C ion beams could still demonstrate (sub)millimeter reproducibility when comparing the distal activity distributions of measurements from different treatment fractions, accuracy studies based on the comparison of the measured activity with a prediction typically obtained from full blown Monte Carlo calculations were typically limited to an agreement of 1–5 mm [25]. However, such results were generally felt still unsatisfactory for routine clinical exploitation. The reasons could be partly attributed to uncertainties in the prediction models, particularly in terms of the knowledge of nuclear interaction cross sections, tissue composition (especially relevant for the prediction of activity distributions dominated by target fragmentation) as well as washout processes (particularly pronounced in the offline studies), along with shortcoming of the in-room/offline PET implementation and suboptimal performances of commercial nuclear medicine scanners when used outside their original field of application. In fact, reconstruction of very weak and broad activity distributions from a mixture of isotopes is more challenging than in the case of localized, intense activity sources of single isotopes, as typical in radiotracer imaging. On the other hand, development of PET systems tailored to the requirements of treatment monitoring in ion beam therapy can be time demanding and costly, explaining the sparsity of attempts to overcome the limitations encountered in the first investigations relying on established detector components of nuclear medicine systems. Nevertheless, in the last years some groups have engaged in this endeavor, aiming to harness PET detector technologies in the scope of ion beam therapy monitoring. Moreover, new horizons in detector technologies have opened the prospects of novel intriguing imaging applications beyond the visualization of the positron emitter distributions, promising to expand the field

of application beyond the more conventional in-vivo verification of the beam range in the patient, as addressed in the following.

3 Next generation of in-beam PET detector systems under clinical translation

3.1 The INSIDE in-beam dual-head PET scanner for proton and carbon ion therapy monitoring

A novel dual-head PET system exploiting state-of-the-art detector technologies based on solid-state photodetectors and custom front-end electronics has been recently integrated in the horizontal beamline of the Centro Nazionale di Adroterapia Oncologica (CNAO, Italy) and is being deployed in first clinical trials for monitoring tumor treatments with protons [26] and carbon ion [27] beams (Fig. 2). The INSIDE (Innovative Solution for Dosimetry in Hadrontherapy) system consists of two planar heads of $10 \times 25\,cm^2$ active area, featuring 2×5 detection modules with 16×16 Lutetium Fine Silicate (LFS) crystals coupled 1:1 to Hamamatsu silicon photomultipliers (SiPMs) [26]. Special efforts have been undertaken to provide time-resolved analysis of the detected events for an online coincidence finding, to support the ability of the system to reconstruct tiny amounts of detected events during the in-beam operation. In particular, an on-the-fly reconstruction algorithm was shown able to provide usable tomographic images in a proton clinical treatment with a time resolution of ca. 10 s and an average delay of 6 s between the beam delivery and the availability of the reconstructed images [26]. Although also this in-beam PET system is currently exploiting only the signal detected in the pauses of the pulsed delivery from the synchrotron accelerator as in the reported experience at GSI (see section 2), work is ongoing at the data acquisition and data processing level to enable exploitation also of the data retrieved during real beam extraction [27], to overcome the huge background from other radiation (e.g., prompt gamma). Different data evaluation strategies are being also assessed [26,28,29], aiming to provide an automated time-resolved analysis which can support on-the-fly quantitative verification of the applied treatment. The initial results reported for baseline phantom studies and selected clinical cases of an observational trial indicate the ability of the system to monitor the beam range with millimeter accuracy and precision, compatible with the system mechanical accuracy [26,30]. Very recent results reported for all proton therapy patients monitored within the INSIDE clinical trial showed an average range variation standard deviation of about 2.5 mm for patients showing no morphological changes in control CTs, while larger values were found for patients exhibiting small anatomical changes, with

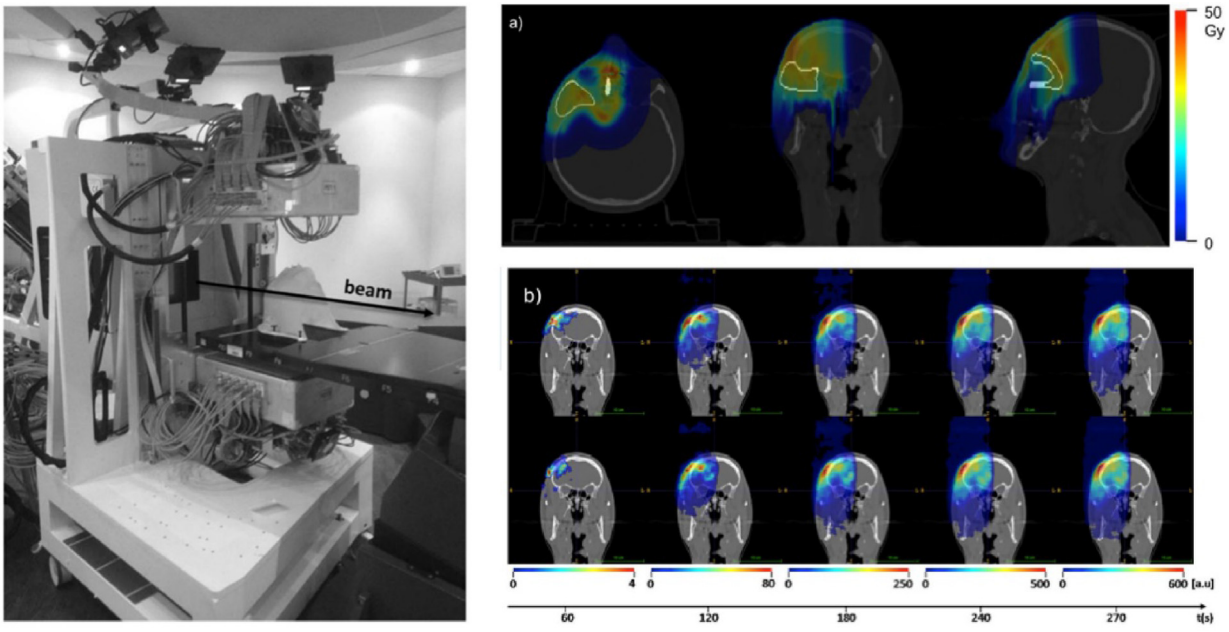

Figure 2. Left: The INSIDE in-beam dual-head PET scanner at CNAO, resting on a mobile support placed between the horizontal beam line nozzle (with beam direction indicated by an arrow) and the patient couch. Right: a) Proton treatment plan displaying the colour-coded dose overlaid on different views of the patient CT, indicating the clinical target volume in white. b) Time evolution of the colour-coded irradiation induced activity, shown in a 2D slice again superimposed to the planning CT for two different treatment fractions (top and bottom row). Taken from [26].

a good correlation between the PET-based range observations and the morphological changes in the CTs [29]. Future analysis including also the results for the carbon ion patients cohort will enable assessing whether the dedicated efforts to tailor the PET imaging system to the peculiar needs of particle therapy monitoring can improve the quality of the treatment verification for routine application in comparison to the previous experience. Moreover, the timing ability of the system could also support ongoing investigations which postulate the usability of the signal from very short-lived (in the millisecond time scale) emitters such as ^{12}N to provide "beam-on" information [31], aiming to bring PET monitoring a step closer to a "real-time" detection and thus compete with the other prompt signatures being explored especially in the context of proton range verification (see comprehensive review in [25]), such as prompt gamma imaging [32,33]. Moreover, the in-beam PET system at CNAO could be operated simultaneously to another detector technology relying on the acquisition of secondary charged particles, so called dose profiler, as particularly focused on the assessment of the transverse beam position [34]. This could not only enable a cross-validation between the outcome of the two independently used monitoring systems, but could also provide new opportunities enabled by the synergistic usage of the two complementary modalities, particularly of interest in the case of carbon ion irradiation where more secondary charged particles can be detected compared to lighter ions/protons.

3.2 OpenPET – full-ring PET geometries for in-beam PET

One of the limitations of a dual-head geometry is the missing resolution performance along the axis perpendicular to the detector planes. Time-of-flight (TOF) information can mitigate the resolution loss, but a few hundred ps TOF resolution in current PET technologies would not be enough [35]. A few tens of ps TOF resolution may enable direct localization without image reconstruction [36,37], but its application to in-beam PET could be still challenging because of the issue of potential radiation damage to front-end circuits, when resorting to highly integrated solutions close to the beam for faster timing detectors.

A practical method to enable artifact-free in-beam PET is OpenPET, which is a PET geometry proposed by a group of National Institutes for Quantum Science and Technology (QST, former NIRS) as a full-ring geometry with an accessible path to an imaging subject. Two possible geometries have been proposed for OpenPET, a dual-ring OpenPET (DROP) [38] and a single-ring OpenPET (SROP) [39]. In DROP, a physically opened field-of-view (FOV), which is made by splitting a detector ring axially, can be imaged by lines-of-response (LORs) between each detector ring. Reconstruction only from oblique LORs results in missing low frequency components [40], but its effect in image reconstruction is smaller than that of missing projection views which is the case of a dual-head geometry. However, twice the number of detectors is required for DROP, which also results in an extension of the axial FOV [41]. The SROP has been proposed to overcome such limitations of DROP. SROP is a single cylinder geometry, but both ends of the cylinder are cut by two parallel aslant planes.

The key detector technology that enabled these OpenPET systems is a depth-of-interaction (DOI) measurement capability. Even for high density scintillators dedicated for PET application, the scintillators should be around 20 mm thick enough to maintain efficiency, and spatial resolution loss due to the thickness of scintillators, often referred as the parallax error, occurs for gamma-rays incoming with an angle. Therefore, the DOI detection, which is the measurement of three-dimensional interaction points inside the scintillator block, is mandatory to keep adequate spatial resolution in the open FOV. Human-sized prototypes have been made for each OpenPET geometry with 4-layered DOI detectors (Fig. 3). In order to reduce background activity for weak activity imaging, Zr-doped gadolinium oxorthosilicate GSO (Gd_2SiO_5) scintillators (GSOZ) [42], which have less natural radioactivity, were selected. Each scintillator was sized in crystals of $2.8 \times 2.8 \times 7.5$ mm^3 dimension, and the DOI block consisted of an array of $16 \times 16 \times 4$ (DOI layer) crystals. In order to overcome the issue of potential radiation damage, photomultiplier tubes (PMTs) were selected as photodetectors rather than silicon photomultipliers (used e.g., by the INSIDE scanner), since the latter were not so tolerant to radiation damage when they first appeared on the market, especially in the case of carbon ion irradiation. Also 15-m long cables were used to locate digitizer circuits away from the irradiation field. The developed DROP and SROP are used for in-beam studies with phantoms and animals at the Heavy Ion Medical Accelerator in Chiba (HIMAC) [43,44].

3.3 Jagiellonian PET – a portable and reconfigurable PET from plastic scintillators with capabilities of ion therapy monitoring

Jagiellonian PET (J-PET) is being developed at the Jagiellonian University in Cracow as a cost-effective technology for positron emission tomography [45] with the potential for in-beam treatment monitoring in ion beam therapy [46]. The J-PET detection system is constructed from the axially arranged plastic scintillator strips read out at both ends by SiPMs [47–49]. Plastic scintillators are more than one order of magnitude less expensive than crystals used in the current PET systems [50], and they provide more than one order of magnitude faster signals (with decay time of

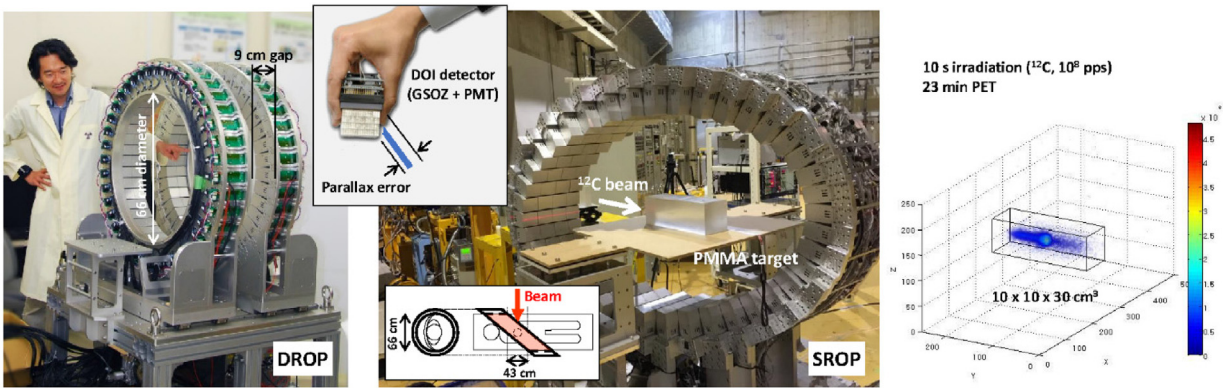

Figure 3. Prototypes of dual-ring Open PET (DROP) and single-ring OpenPET (SROP). Spatial resolution loss in the open field-of-view due to the parallax error is mitigated by the use of a depth-of-interaction (DOI) detector. An example of phantom imaging results for a carbon pencil beam with 10^8 particle per second (pps) is shown, where only in 10 s of irradiation followed by 23 min of PET acquisition with the setup shown in the middle panel it is possible to visualize with good quality the activation of a homogenous PMMA phantom.

about 2 ns compared for example to 40 ns of LYSO or 300 ns of BGO crystals) [49]. These advantageous timing properties with fast decaying signals (less prone to pile-ups and saturation in high irradiation rate environment) open new opportunities in the context of in-beam monitoring. This is despite the known shortcomings of plastic scintillators such as low detection efficiency and moderate light output, which as shown in references [48–50] may be compensated by the multi-layer and long axial field-of-view systems. Moreover, plastics scintillators are light, enabling robust and lightweight construction, contrary to the fragile crystal scintillators. Fig. 4 presents photographs of the latest J-PET prototype consisting of 24 independent detection modules which can be easily reconfigured and transported. The full system with 50 cm axial field-of-view weights only 60 kg and its shape can be tailored to the clinical needs. Both the cylindrical and dual-head configurations have been already successfully commissioned for the clinical examinations with patients in the hospital (left panel of Fig. 4), and for tests of proton beam range monitoring with phantoms (right panel of Fig. 4). The modular J-PET is equipped with a dedicated trigger-less data acquisition system [52] provid-

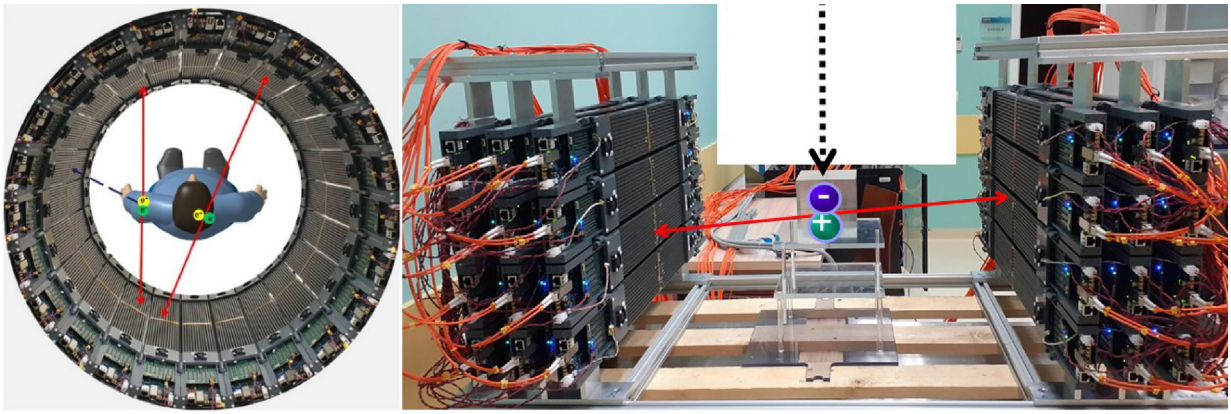

Figure 4. Photographs of two possible settings for the modular and reconfigurable J-PET prototype consisting of 24 detection modules. Each module comprises 13 scintillator strips with the length of 50 cm and cross section of 6 mm × 24 mm. Each scintillator strip is read out by 8 SiPMs, 4 at each end. Electric signals from SiPMS are digitized by dedicated front-end electronics visible in the foreground [51]. Left panel: Cylindrical configuration with the superimposed presentation of positron-electron annihilations in the patient's body. Red solid arrows indicate annihilation photons, and the blue dashed arrow shows the prompt gamma (γ) emitted by the $\beta^+\gamma$ radionuclide such as e.g. ^{14}O. Right panel: Photograph taken during the tests conducted in the Cracow Proton Therapy Center. An exemplary dual-head configuration with 4 × 3 modules set at each side of the irradiated object is shown. Arrangement of detection modules in three layers compensates for the low efficiency of plastic scintillators. Red solid arrows indicate annihilation photons from the electron positron annihilation in the phantom irradiated by the proton beam (dashed arrow).

ing the possibility of multi-photon imaging [12,53]. An example of multi-photon event (i.e., detection of photons originating from different mechanisms, such as nuclear deexcitation vs positron annihilation) is shown in the left panel of Fig. 4. An event demonstrated pictorially on the left shoulder indicates an example of emission of prompt gamma (γ) from the decay chain of $^{14}O \rightarrow {}^{14}N^{*}\ e^{+}\ \nu \rightarrow {}^{14}N\ \gamma\ e^{+}\ \nu$, followed by the positron–electron ($e^{+}e^{-}$) annihilation into two photons (red arrows). The potential of multi-photon imaging beyond treatment monitoring will be introduced in chapter 3.4.2 in relation to the prospects for imaging positronium properties which are sensitive to the intra-molecular environment and concentration of oxygen in the tissue [15]. This may become useful in providing information about the degree of the tumor hypoxia [54,55], which can also be greatly relevant to ion beam therapy.

3.4 Augmenting the abilities of conventional PET imaging

3.4.1 Whole Gamma Imaging

The potential of PET can be augmented with the help of Compton camera imaging. This novel concept of PET combined with Compton imaging is referred in the literature as γ-PET [10] or whole gamma imaging (WGI) [11]. Different from the multi-photon imaging based on the timing performance of a single PET ring (see section 3.3), in WGI an additional detector ring, which is used as the scatterer, is inserted in a conventional PET ring so that single gamma rays can be detected by the Compton imaging method. Simultaneous PET imaging is still possible by the coincidence detection in the PET ring as well as the coincidence in the scatterer or the coincidence between the PET ring and the scatterer. Further large impact can be expected for triple gamma emitters such as ^{44}Sc (about 4 h half-life), that emits a positron and a 1157 keV gamma ray almost at the same time [56]. In principle, only a few decays would be enough to localize the source position by calculating intersection points of a 511 keV LOR with a 1157 keV Compton cone.

A prototype of the WGI system has been developed in QST [11] (Fig. 5). The 4-layer DOI detector that was used for OpenPET is used for the absorber, i.e., the PET ring. A total of 160 detectors were used to form four rings each with a diameter of 66 cm. The ring diameter of the scatterer was 20 cm, and in total, 40 detector blocks were used to form two rings. As high energy resolution is required in Compton imaging, gadolinium aluminum gallium garnet (GAGG) was selected as a bright scintillator with acceptable stopping power. Each scatterer detector consisted of a 24×24 array of GAGG crystals ($0.9 \times 0.9 \times 6.0\ mm^3$ each) coupled with an 8×8 SiPM array (Hamamatsu S14161-3050HS-08). All interaction events were recorded as list-mode data, and event selection such as coincidence detection was done by software in post-processing.

A ^{137}Cs point source was measured to evaluate the Compton imaging performance, and the spatial resolution obtained by 3D list-mode ordered subset expectation maximization (OSEM) was 4.4 mm FWHM (8 cm off-center) - 13.1 mm FWHM (center). The WGI prototype was also assessed by using a ^{89}Zr source (half-life = about 3.27 days). ^{89}Zr emits a 909 keV single-gamma ray as well as a positron, and direct comparison of Compton imaging of 909 keV photons with PET is possible [57]. A small rod phantom experiment showed that the WGI Compton imaging had spatial resolution better than 3.0 mm at the peripheral region although the center region had lower resolution due to the larger uncertainties in reconstructing the Compton kinematics. PET resolved 2.2 mm rods clearly at any location. A mouse 1 d after injection of 9.8 MBq ^{89}Zr oxalate was measured for 1 h, and the Compton imaging result agreed well with the PET image.

The ^{22}Na point source which emits a 1275 keV gamma ray immediately after a positron decay was also used to demonstrate the triple gamma mode, i.e., the simultaneous exploitation of the Compton cone of the prompt gamma and the line-of-response of the annihilation photons. Spatial resolution values for the ^{22}Na point source, obtained by the absorber-absorber coincidence and the scatterer-scatterer coincidence, were almost the same (below 2 mm). In the triple gamma mode, where only simple backprojection was used and no image reconstruction algorithm was applied, spatial resolution for the ^{22}Na point source was 4.8 mm FWHM (8 cm off-center) – 5.7 mm FWHM (center). ^{44}Sc was produced as a practical candidate of the non-pure positron emitters, and 6.6 mm FWHM (center) and 5.8 mm FWHM (8 cm off-center) were obtained in the same manner for a vial. Improvement in energy resolution of the scatterer detector is required to obtain better spatial resolution. WGI with ^{44}Sc can be also used to measure positronium lifetime, which is described in the next sub-section.

3.4.2 Positronium imaging

Monitoring of ion beam therapy with PET systems utilizes information about the density distribution of electron-positron annihilations correlated with the density distribution of β^{+}-radionuclides produced by ions in the nuclear reactions, which in turn is correlated with the spatial distribution of the deposited ionization dose in the patient's body. In the current PET systems this information is extracted based on the registration of electron-positron annihilations into two photons. However, positron annihilation can also provide information about the molecular environment in which it annihilates [15]. Recently, with the newly invented positronium imaging [12–14,58] and multi-photon J-PET system [53] (see section 3.3), it was demonstrated that it is possible

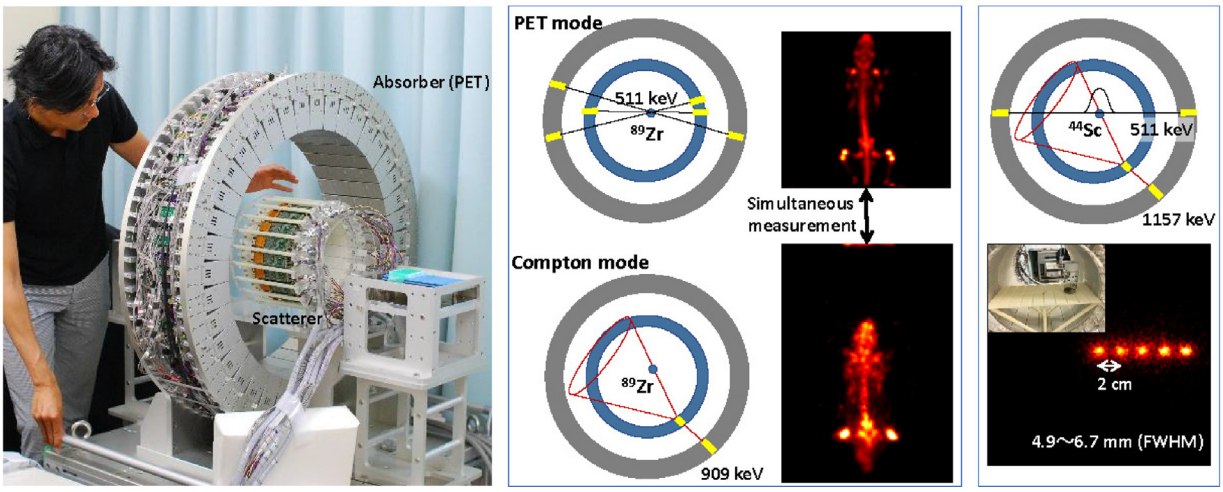

Figure 5. A demonstration of whole gamma imaging (WGI), which combines PET with Compton imaging. For ^{89}Zr, which emits a 909 keV gamma-ray and a positron with a time interval, the same mouse was imaged in two different modes: a PET mode and a Compton mode. For ^{44}Sc, which emits a 1157 keV prompt gamma-ray after a positron decay, a feasibility of reconstruction-less localization as an intersection point between the line-of-response and a surface of the Compton cone was shown.

to gain information not only about the positron annihilations density distribution but also about the size of the intra-molecular voids and concentration in them of oxygen molecules [15,54,55]. The multi-photon imaging capabilities of the J-PET system enable to detect, in a single event, two- or three-photons from electron-positron annihilations (e+e- -> photons) and also prompt gamma from the deexcitation of the radionuclide. The registration of prompt gamma (γ) emitted e.g. in the decay chain of ^{44}Sc isotope (^{44}Sc $\rightarrow$ ^{44}Ca* e^+ ν $\rightarrow$ ^{44}Ca γ e^+ ν) enables to determine the time at which positron (e+) is emitted into the tissue, while the time of the registration of annihilation photons (e+e- -> photons) is used to determine the time of positron-electron annihilation in the tissue. On the average the deexcitation of ^{44}Ca* takes place in 2.6 ps, and the delay between the emission of positron and prompt gamma can be safely neglected in the calculations [12]. An application of multi-photon data acquisition of the J-PET and fast timing of plastic scintillators enabled to determine first ex-vivo images of positronium lifetime in cancer and healthy tissues operated from the patients [14].

In the human body the positron-electron annihilation proceeds via formation of the positronium atom in about 40% cases [14,15], and in about 60% cases the positron emitted by the radionuclide annihilates in the tissue directly (predominantly into two photons). The left panel of Fig. 6 illustrates the main processes leading to the positron annihilations in the example of the CD44 molecule which is present in glioblastoma tumour, one of the cancers qualified for ion beam therapy. In a quarter of cases positronium is formed as a short-lived para-positronium decaying predominantly into two photons (with the mean lifetime in vacuum of 125 ps), and in three-quarter of cases as a long-lived ortho-positronium decaying mainly into three photons (with the mean lifetime in vacuum of 142 ns).

The mean lifetime of ortho-positronium produced in the intra-molecular voids is significantly shortened due to the pick-off processes in which positron from positronium annihilates with the electrons from the surrounding atoms and due to the conversion processes on para-magnetic molecules (as e.g. oxygen) in which ortho-positronium converts into para-positronium. Therefore, the smaller the intra-molecular voids are, the shorter is the ortho-positronium lifetime, and the higher the oxygen concentration, the shorter the ortho-positronium lifetime is. Moreover, the ratio of three-photon to two-photon annihilation rates is also decreasing with the growth of the oxygen concentration and with the decrease of the void size. Therefore, information which may be extracted from the image of mean positronium lifetime and from the image of the ratio of three-photon to two-photon annihilation rate may enable to assess the tissue pathology at the early stage of molecular alterations [14,59] and to assess the degree of hypoxia [54,55]. Hypoxia is referred to as the condition in which the oxygen concentration in the tissue is insufficient for the normal course of physiological processes. The right panel of Fig. 6 shows that the partial pressure of oxygen differs between healthy and cancer tissues and varies from 10 mmHg for brain up to 50 mmHg for pancreas. Hypoxia increases resistance to radiation therapy because at lower oxygen concentrations, levels of radiation-induced reactive oxygen species (ROS) are lower, leading to less oxidative

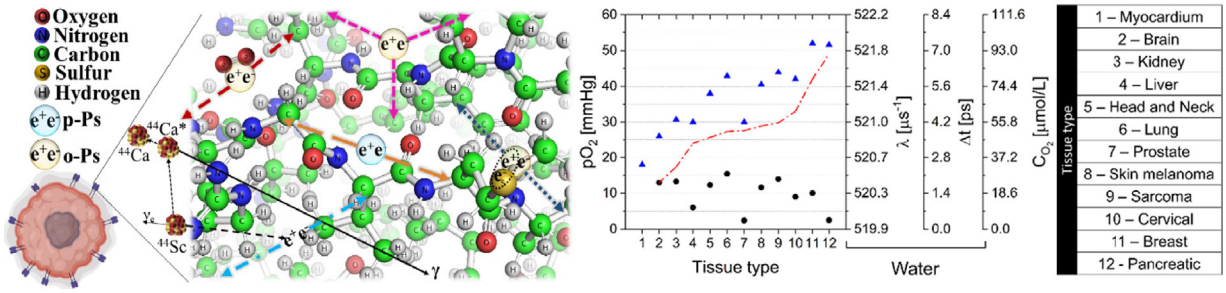

Figure 6. Left panel: Illustration of processes of positron-electron annihilation in the CD44 molecule present in the glioblastoma tumor. It may annihilate directly into two photons (blue dashed arrows) or it may form a metastable short-lived para-positronium (blue) or long-lived ortho-positronium (yellow). Para-positronium decays into two photons (dashed brown arrows), while ortho-positronium self-annihilates into three photons (dashed violet arrows) or into two-photons via pick-off process (blue dotted arrows) or via conversion on the oxygen molecules into para-positronium (dashed claret arrows). Right panel: Partial pressure of oxygen in tumor (black circles) and healthy tissues (blue triangles) shown for various tissue types as explained in the legend [54]. The data are ordered according to the increasing value of a difference between the oxygen partial pressure for healthy and cancer tissues (dashed-dotted line). Right axes show the corresponding decay constant (λ), changes in the mean ortho-positronium lifetime (Δt) and the oxygen concentration (C_{O2}).

damage to the DNA and therefore less effective killing of cancer cells [60]. Therefore, monitoring the degree of hypoxia by imaging of positronium properties in the irradiated tissues would enable more precise and personalized ion beam therapy planning. Recently, it was argued that with the current timing resolution and advent of multi-photon PET systems [14,53] positronium can serve as a biomarker of hypoxia [54,55]. First ortho-positronium lifetime [14] and three-photon [53] images were demonstrated by means of the J-PET tomograph. For the lifetime image the prompt photon is used to determine the time when the positronium is produced and annihilation photons inform about the positronium decay. So, for positronium lifetime, only these radionuclides may be used which emit prompt gamma (as e.g. ^{10}C and ^{14}O), while the three-photon to two-photon rate ratio may be imaged for all kinds of β^+-emitters.

The resolution of the mean positronium lifetime determination depends predominantly on the value of the mean positronium lifetime (τ) [58] which in the tissue varies between about 1.8 ns in water to about 4 ns in the skin [14]. The variance of the exponential distribution of the lifetime (1/τ e^-(t/τ)) is equal to τ^2. Therefore, the resolution expressed as a standard deviation scales as τ/sqrt(N), where N is the number of registered events. In the first ex-vivo images 20 ps resolution was indeed

achieved [14]. In proton therapy the target volume is irradiated with 10^{10} to 10^{11} protons that may lead to the production of about 10^6 to 10^7 of ^{10}C or ^{14}O radionuclides ($\sim 10^{-4}$ of ^{14}O per proton [61]). Thus, the scanner with the efficiency of 1% for the registration of three-photon events (as e.g. J-PET [62]) could enable determination of annihilation lifetime with the precision in the order of 10 ps. Even higher resolution could be expected when applying radioactive beams of ^{10}C or ^{14}O, as discussed in the next section.

3.5 Prospects of radioactive ion beams for imaging and therapy

One of the limitations in PET-based range verification is the intrinsic difference between the PET signal (activity peak for ions able to produce β+-emitting projectile fragments, distal fall-off otherwise) and the Bragg peak, and properly accounting for this difference is challenging because the difference is object- and ion-dependent. The best scenario is to change a treatment beam itself to positron emitters such as ^{11}C and ^{15}O ions, which are referred to as radioactive ion (RI) beams. ^{10}C and ^{14}O can be also used as an RI beam. Partial use of RI beams, as initially conceived in the pioneering experience of ion beam therapy at the Lawrence Berkeley Laboratory [8], may sound more practical: a pencil RI beam with very low intensity is used before the treatment with conventional stable beams just to verify the range point-by-point, especially for edge regions of the tumour very close to organs at risk. Moreover, advances in accelerator technologies can raise new prospects of sufficiently intense RI beams for imaging and treatment simultaneously [63].

Fig. 7 compares a simulated positron emitter distribution produced by a stable ^{12}C ion beam with that of RI beams of ^{11}C and ^{10}C. Even in RI beam irradiation, positron emitters are produced as fragments, but those are almost negligible compared with the activity of the primary beam particles not undergoing nuclear fragmentation and thus reaching their deepest stopping position. Therefore, PET imaging of RI beams can provide exact location of such prominent stopping position, which is highly correlated to the Brag peak position [9]. In the comparison between ^{11}C (about 20 min half-life) and ^{10}C (about 19 s half-life), it is obvious that for the same number of implanted ions a shorter half-life

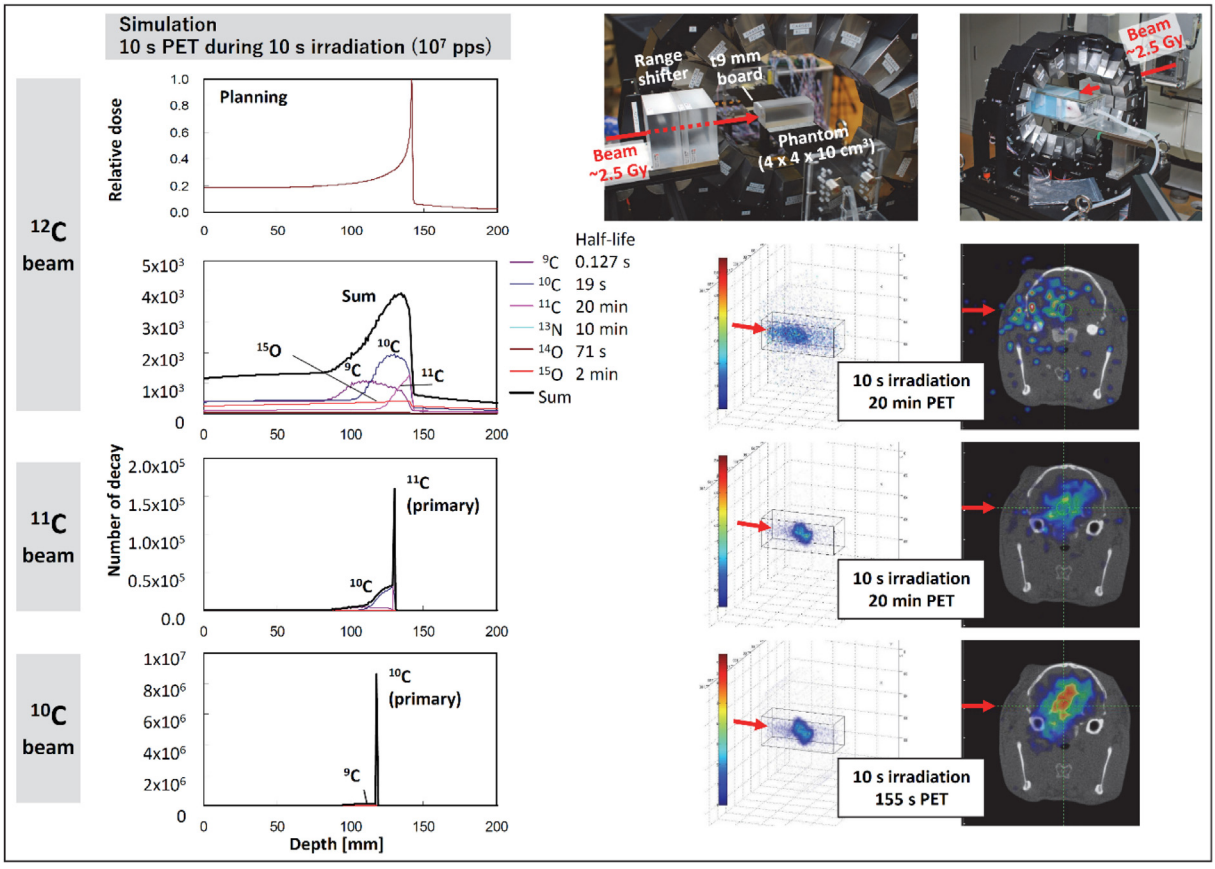

Figure 7. Comparison of PET imaging for a stable ^{12}C ion beam with radioactive ion (RI) beams of ^{11}C and ^{10}C. A positron emitter distribution clearly reflecting the beam stopping position is obtained with the RI beams (left, simulation), in contrast to the stable beam irradiation. A 9 mm difference introduced at the Bragg peak position by inserting a range shifter covering only half of the beam is clearly observed in the OpenPET images with the RI beams (middle, experiment). An OpenPET study for irradiation of a rabbit also demonstrates improved treatment monitoring with RI beams (right, experiment).

results in higher activity. In HIMAC, various RI beams are available for physics experiment, and their suitability for range verification depends on their abundance (related to their production rate) and half-life (with the shortest half-life given rise to the strongest activity signal). For example, ^{11}C and ^{10}C beams are made from a ^{12}C beam by using a Be target. In in-beam phantom studies with a small OpenPET prototype [64], a 9-mm difference in the Bragg peak position created by insertion of a range shifter covering only half of the beam was clearly observed in the RI beams, whereas it was not clearly seen with the stable ^{12}C beam. The concept of RI beam irradiation was also shown in rabbit studies, where it was possible to confirm the beam delivery to the center of the brain by the OpenPET when using RI beams. However, one of the limitations in the current technologies is the quality of RI beams generated as a secondary beam; the beam intensity is ∼1/1000 in ^{11}C and ∼1/10000 in ^{10}C compared with the original ^{12}C beam. Also, the RI beams generated as a secondary beam tend to have blurred energy distribution, and more sharpened beams can be only obtained at the cost of more reduced beam intensity.

As explored in pioneering studies at HIMAC in the early 2000s, in living tissue only a fraction of the implanted positron activity (about one third for a rabbit thigh muscle [65]) can be used for imaging and the rest is washed out of the target area. Whereas this is typically seen as a challenge for treatment monitoring, as it reduces the signal correlated to the initial dose deposition, the clearance rate of RI beams due to the biological washout effect can also be used as a new biomarker [66]. In a conventional stable beam irradiation, the analysis of the washout speed is challenging because various radiolabeled (such as ^{11}C-labeled and ^{15}O-labeled) chemical compounds are contaminated in PET images, in addition to the very low activity level of the irradiation-induced fragments. In contrast, in the case of RI beams, a single radionuclide with a high signal-to-noise ratio

can be tracked by PET imaging. So far, it has been shown that the tumor vascular status in rats can be observed by analyzing the washout rates in ^{15}O in-beam PET [67]. There is one more possible extension of these studies for the ^{10}C RI beam, because ^{10}C emits a 718 keV prompt gamma ray after a positron decay. This indicates that the ^{10}C distribution can be visualized by means of WGI. The first in-beam WGI measurement of a phantom irradiated by a ^{10}C beam has been carried out at QST [68].

In addition to the pioneering activities at HIMAC, more research on the use of RI beams for imaging and treatment is currently ongoing in the framework of the BARB (Biomedical Applications of Radioactive ion Beams) project, aiming to leverage the intensity upgrade of the FAIR/GSI accelerator in order to demonstrate the potential advantages of RI beams in ion beam therapy [66]. To this end, preclinical experiments in small animal tumour models will aim at demonstrating the expected benefits from improved targeting accuracy and reduced margins achievable with RI beams, along with their potential to act as in-vivo tracers to clarify the role of vascular damage in single-fraction high-dose radiotherapy [66]. These experiments will rely on a novel high-sensitivity and high-resolution in-beam PET scanner developed in the context of a small animal irradiator prototype platform [69,70], planned to be upgraded with Compton imaging capabilities toward WGI operation [71].

Conclusion and outlook

Ninety years after the discovery of the positron, unconventional application of PET imaging to in-vivo monitoring of ion beam therapy with stable and radioactive beams continues to be a vivid topic of research. Building upon the experience generated by first systems mostly adapted from conventional nuclear medical imaging, recent advances in detector technologies and data processing promise enhanced performances for reliable monitoring of the in-vivo beam range, to foster improved targeted accuracy for more efficient tumor eradication with reduced burden to the normal tissue. Moreover, recent experiments with advanced prototype systems showed the promising possibility to augment the PET imaging abilities toward utilization of all irradiation-induced energetic photon emissions for combined PET and Compton imaging, along with the visualization of the positronium lifetime in multi-photon imaging. Together with the advancement of accelerator technologies which may now enable the production of intense RI beams, all these new developments open intriguing prospects which might not only benefit the physical conformation of ion beam therapy, but also shed novel insights in biological mechanisms to be exploited for more effective localized treatment in personalized therapy.

Declaration of Competing Interest

The authors declare that they have no known competing financial interests or personal relationships that could have appeared to influence the work reported in this paper.

Acknowledgments

Pawel Moskal would like to thank D. Panek and Sz. Parzych for help with preparation of figures. The authors acknowledge support by the Japan Society for the Promotion of Science (JSPS) KAKENHI Grants (20H05667 and 21K19936), the QST Future Laboratory Program, Nakatani Foundation in Japan, the Foundation for Polish Science via TEAM POIR.04.04.00-00-4204/17 program, the NCN grant no. 2021/42/A/ST2/00423, the SciMat and qLife Priority Research Areas budget under the program *Excellence Initative - Research University* at the Jagiellonian University, as well as the European Research Council (grant numbers 725539 and 883425).

References

[1] Jäkel O. Physical advantages of particles: protons and light ions. Br J Radiol 2020;93:20190428.
[2] Karger CP, Peschke P. RBE and related modeling in carbon-ion therapy. Phys Med Biol 2018;63:01TR02.
[3] Paganetti H. Range uncertainties in proton therapy and the role of Monte Carlo simulations. Phys Med Biol 2012;57:R99.
[4] Parodi K. On the feasibility of dose quantication with in-beam PET data in radiotherapy with ^{12}C and proton beams, PhD thesis, Dresden University of Technology; 2004 (in Forschungszentrum Rossendorf Wiss-Techn-Ber FZR-415, 2004).
[5] Priegnitz M, Möckel D, Parodi K, Sommerer F, Fiedler F, Enghardt W. In-beam PET measurement of 7Li3+ irradiation induced beta+-activity. Phys Med Biol 2008;53:4443.
[6] Pawelke J, Bortfeld T, Fiedler F, Kluge T, Möckel D, Parodi K, et al. Therapy monitoring with PET techniques, Proceeding of the 39. Annual Conference of the German-Swiss Association for Radiation Protection and 11th Workshop of Heavy Charged Particles in Biology and Medicine, Heidelberg, 2007, ISSN 1013-4506
[7] Bauer J, Tessonnier T, Debus J, Parodi K. Offline imaging of positron emitters induced by therapeutic helium, carbon and oxygen ion beams with a full-ring PET/CT scanner: experiments in reference targets. Phys Med Biol 2019;64:225016.
[8] Llacer J. Positron emission medical measurements with accelerated radioactive ion beams. Nucl Sci Appl 1988;3:111–131.
[9] Mohammadi A, Tashima H, Iwao Y, Takyu S, Akamatsu G, Kang HG, et al. Influence of momentum acceptance on range monitoring of 11 C and 15 O ion beams using in-beam PET. Phys Med Biol 2020;65:125006.
[10] Lang C, Habs D, Parodi K, Thirolf PG. Sub-millimeter nuclear medical imaging with high sensitivity in positron emission tomography using β+γ coincidences. JINST 2014;9:P01008.
[11] Yoshida E, Tashima H, Nagatsu K, Tsuji AB, Kamada K, Parodi K, et al. Whole gamma imaging: a new concept of PET combined with Compton imaging. Phys Med Biol 2020;65:125013.

[12] Moskal P et al.. Feasibility study of the positronium imaging with the J-PET tomograph. Phys Med Biol 2019;64:055017.
[13] Moskal P. Positronium imaging. In: 2019 IEEE Nuclear Science Symposium and Medical Imaging Conference (NSS/MIC). Manchester, UK: IEEE Xplore; 2020.
[14] Moskal P, Dulski K, Chug N, Curceanu C, Czerwiński E, Dadgar M, et al. Positronium imaging with the novel multiphoton PET scanner. Science. Advances 2021;7:eabh4394. https://doi.org/10.1126/sciadv.abh439.
[15] Moskal P, Jasińska B, Stępień EŁ, Bass S. Positronium in medicine and biology. Nat Rev Phys 2019;1:527.
[16] Maccabee HD, Madhvanath U, Raju MR. Tissue activation studies with alpha-particle beams. Phys Med Biol 1969;14:213–224.
[17] Tobias CA, Benton EV, Capp MP, Chatterjee A, Cruty MR, Henke RP. Particle radiography and autoactivation. Int J Radiat Oncol Biol Phys 1977;3:35.
[18] Bennett GW, Archambeau JO, Archambeau BE, Metzer JI, Wingate CL. Visualization and transport of positron emission from proton activation in vivo. Science 1978;200:1151–1153.
[19] Enghardt W, Crespo P, Fiedler F, Hinz R, Pawelke J, Parodi K. Pönisch F Charged hadron tumour therapy monitoring by means of PET. Nucl Instrum Methods A 2004;525:284–288.
[20] Enghardt W, Parodi K, Crespo P, Fiedler F, Pawelke J, Pönisch F. Dose quantification from in-beam positron emission tomography. Radiother Oncol 2004;73:S96.
[21] Crespo P, Shakirin G, Enghardt W. On the detector arrangement for in-beam PET for hadron therapy monitoring. Phys Med Biol 2006;51:2143–2163.
[22] Shakirin G, Braess H, Fiedler F, Kunath D, Laube K, Parodi K, et al. Implementation and workflow for PET monitoring of therapeutic ion irradiation: a comparison of in-beam, in-room, and off-line techniques. Phys Med Biol 2011;56:1281.
[23] Knopf A, Parodi K, Bortfeld T, Shih HA, Paganetti H. Systematic analysis of biological and physical limitations of proton beam range verification with offline PET/CT scans. Phys Med Biol 2009;54:4477.
[24] Crespo P, Barthel T, Frais-Kölbl H, Griesmayer E, Heidel K, Parodi K, et al. Enghardt W Suppression of random coincidences during in-beam PET measurements. IEEE Trans NuclSci 2005;52:980–987.
[25] Parodi K. In Vivo Treatment Verification, in Proton Therapy Physics, Second Edition, edited by Harald Paganetti. CRC Press; 2018.
[26] Ferrero V, Fiorina E, Morrocchi M, Pennazio F, Baroni G, Battistoni G, et al. Bisogni MG Online proton therapy monitoring: clinical test of a Silicon-photodetector-based in-beam PET. Sci Rep 2018;8:4100.
[27] Kostara E, Sportelli G, Belcari N, Camarlinghi N, Cerello P, Del Guerra A, et al. Particle beam microstructure reconstruction and coincidence discrimination in PET monitoring for hadron therapy. Phys Med Biol 2019;64:035001.
[28] Kraan AC, Berti A, Retico A, Baroni G, Battistoni G, Belcari N, et al. Localization of anatomical changes in patients during proton therapy with in-beam PET monitoring: A voxel-based morphometry approach exploiting Monte Carlo simulations. Med Phys 2022;49:23.
[29] Moglioni M, Kraan AC, Baroni G, Battistoni G, Belcari N, et al. In-vivo range verification analysis with in-beam PET data for patients treated with proton therapy at CNAO. Front Oncol 2022.
[30] Pennazio F, Battistoni G, Bisogni MG, Camarlinghi N, Ferrari A, Ferrero V, et al. Carbon ions beam therapy monitoring with the INSIDE in-beam PET. Phys Med Biol 2018;63:145018.
[31] Buitenhuis HJT, Diblen F, Brzezinski KW, Brandenburg S, Dendooven P. Beam-on imaging of short-lived positron emitters during proton therapy. Phys Med Biol 2017;62:4654–4672.
[32] Berthold J, Khamfongkhruea C, Petzoldt J, Thiele J, Hölscher T, Wohlfahrt P, et al. First-In-Human Validation of CT-Based Proton Range Prediction Using Prompt Gamma Imaging in Prostate Cancer Treatments. Int J Radiat Oncol Biol Phys 2021;111:1033–1043.
[33] Tattenberg S, Marants R, Niepel KB, Bortfeld TR, Sudhyadhom A, Landry G, et al. Validation of prompt gamma spectroscopy for proton range verification in tissue-mimicking and porcine samples. Phys Med Biol 2022. https://doi.org/10.1088/1361-6560/ac950f, Online ahead of print.
[34] Fischetti M, Baroni G, Battistoni G, Bisogni G, Cerello P, Ciocca M, et al. Inter-fractional monitoring of 12C ions treatments: results from a clinical trial at the CNAO facility. Sci Rep 2020;10:20735.
[35] Surti S, Zou W, Daube-Witherspoon ME, McDonough J, Karp JS. Design study of an in situ PET scanner for use in proton beam therapy. Phys Med Biol 2011;56:2667–2685.
[36] Lecoq P, Morel C, Prior JO, Visvikis D, Gundacker S, Auffray E, et al. Roadmap toward the 10 ps time-of-flight PET challenge. Phys Med Biol 2020;65:21RM01.
[37] Kwon SI, Ota R, Berg E, Hashimoto F, Nakajima K, Ogawa I, et al. Ultrafast timing enables reconstruction-free positron emission imaging. Nat Photonics 2021;15:914–918.
[38] Yamaya T, Inaniwa T, Minohara S, Yoshida E, Inadama N, Nishikido F, et al. A proposal of an open PET geometry. Phys Med Biol 2008;53:757–773.
[39] Tashima H, Yamaya T, Yoshida E, Kinouchi S, Watanabe M, Tanaka E. A single-ring OpenPET enabling PET imaging during radiotherapy. Phys Med Biol 2012;57:4705–4718.
[40] Tashima H, Yamaya T, Kinahan PE. An OpenPET scanner with bridged detectors to compensate for incomplete data. Phys Med Biol 2014;59:6175–6193.
[41] Yamaya T, Yoshida E, Inadama N, Nishikido F, Shibuya K, Higuchi M, et al. A multiplex "OpenPET" geometry to extend axial FOV without increasing the number of detectors. IEEE Trans Nucl Sci 2009;56:2644–2650.
[42] Shimizu S, Sumiya K, Ishibashi H, Senguttvan N, Redkin BS, Ishii M, et al. Effect of Mg-, Zr-, and Ta-doping on scintillation properties of Gd2SiO5: Ce crystal. IEEE Trans Nucl Sci 2003;50:778–781.
[43] Yoshida E, Tashima H, Shinaji T, Shimizu K, Wakizaka H, Mohammadi A, et al. Development of a whole-body dual ring OpenPET for in-beam PET. IEEE Trans Rad Plas Med Sci 2017;1:293.
[44] Tashima H, Yoshida E, Iwao Y, Wakizaka H, Mohammadi A, Nitta M, et al. Development of a multiuse human-scale single-ring OpenPET system. IEEE Trans Rad Plas Med Sci 2021;5:807.
[45] Moskal P, Stępień EŁ. Prospects and clinical perspectives of total-body PET imaging using plastic scintillators. PET Clinics 2020;15:439.
[46] Rucinski A, Baran J, Garbacz M, Pawlik-Niedzwiecka M, Moskal P. Plastic scintillator based PET detector technique for proton therapy range monitoring: A Monte Carlo study. 2018 IEEE Nuclear Science Symposium and Medical Imaging Conference, NSS/MIC 2018 - Proceedings' pp. 24–27.
[47] Moskal P, Sz N, Bednarski T, Czerwiński E, Kapłon Ł, Kubicz E, et al. Test of a single module of the J-PET scanner based on plastic scintillators. Nucl Instr and Meth A 2014;764:317–321.
[48] Moskal P, Rundel O, Alfs D, Bednarski T, Białas P, Czerwiński E, et al. Time resolution of the plastic scintillator strips with matrix photomultiplier readout for J-PET tomograph. Phys Med Biol 2016;61:2025–2047.
[49] Moskal P, Kowalski P, Shopa R, Raczynski L, Baran J, Chug N, et al. Simulating NEMA characteristics of the modular total-body J-PET scanner -an economic total-body PET from plastic scintillators. Phys Med Biol 2021;66:175015.
[50] Vandenberghe S, Moskal P, Karp JS. State of the art in total body PET. EJNMMI Phys 2020;7:35. https://doi.org/10.1186/s40658-020-00290-2.

[51] Pałka M, Strzempek P, Korcyl G, Bednarski T, Sz N, Białas P, et al. Multichannel FPGA based MVT system for high precision time (20 ps RMS) and charge measurement. J Instrum 2017;12:P08001.
[52] Korcyl G, Białas P, Curceanu C, Czerwiński E, Dulski K, Flak B, et al. Evaluation of Single-Chip, Real-Time Tomographic Data Processing on FPGA - SoC Devices. IEEE Trans Med Imaging 2018;37:2526–2535.
[53] Moskal P, Gajos A, Mohammed M, Chhokar J, Chug N, Curceanu C, et al. Testing CPT symmetry in ortho-positronium decays with positronium annihilation tomography. Nat Commun 2021;12:5658.
[54] Moskal P, Stępień EŁ. Positronium as a biomarker of hypoxia. Bio-Algorithms Med-Syst 2021;17:311–319.
[55] Shibuya K, Saito H, Nishikido F, Takahashi M, Yamaya T. Oxygen sensing ability of positronium atom for tumor hypoxia imaging. Commun Phys 2020;3:1–8.
[56] Choiński J, Łyczko M. Prospects for the production of radioisotopes and radiobioconjugates for theranostics. Bio-Algorithms Med-Syst 2021;17:241–257.
[57] Tashima H, Yoshida E, Wakizaka H, et al. 3D Compton image reconstruction method for whole gamma imaging. Phys Med Biol 2020;65:225038.
[58] Moskal P, Kisielewska D, Bura Z, Chhokar J, Curceanu C, Czerwiński E, et al. Performance assessment of the 2gamma positronium imaging with the total-body PET scanners. EJNMMI Phys 2020;7:44.
[59] Moskal P, Kubicz E, Grudzień G, Czerwiński E, Dulski K, Leszczyński B, et al. Developing a Novel Positronium Biomarker for Cardiac Myxoma Imaging. bioRxiv 2021:455285. https://doi.org/10.1101/2021.08.05.455285.
[60] Brahimi-Horn CM, Chiche J, Pouyssegur J. Hyoxia and Cancer. J Mol Med 2007;85:1301–1307.
[61] Dendooven P, Buitenhuis HJT, Diblen F, Heeres PN, Biegun AK, Fiedler F, et al. Corrigendum: Short-lived positron emitters in beam-on PET imaging during proton therapy (2015 Phys. Med. Biol. 60 8923). Phys Med Biol 2019;64:129501.
[62] Baran J, Gajewski J, Pawlik-Niedzwiecka M, Moskal P, Rucinski A. Studies of J-PET detector to monitor range uncertainty in proton therapy, 2019 IEEE Nuclear Science Symposium and Medical Imaging Conference (NSS/MIC), IEEE Xplore 2019, 10.1109/NSS/MIC42101.2019.9059793
[63] Durante M, Parodi K. Radioactive Beams in Particle Therapy: Past, Present, and Future. Front Phys 2020 Aug;28(8):00326. https://doi.org/10.3389/fphy.2020.00326.
[64] Tashima H, Yoshida E, Inadama N, Nishikido F, Nakajima Y, Wakizaka H, et al. Development of a small single-ring OpenPET prototype with a novel transformable architecture. Phys Med Biol 2016;61:1795–1809.
[65] Tomitani T, Pawelke J, Kanazawa M, Yoshikawa K, Yoshida K, Sato M, et al. Washout studies of 11C in rabbit thigh muscle implanted by secondary beams of HIMAC. Phys Med Biol 2003;48:875–889.
[66] Boscolo D, Kostyleva D, Safari MJ, Anagnostatou V, Äystö J, Bagchi S, et al. Super-FRS Experiment Collaboration, Radioactive Beams for Image-Guided Particle Therapy: The BARB Experiment at GSI. Front Oncol 2021 Aug;19(11):737050.
[67] Toramatsu C, Mohammadi A, Wakizaka H, Sudo H, Nitta N, Seki C, et al. Measurement of biological washout rates depending on tumor vascular status in ^{15}O in-beam rat-PET. Phys Med Biol 2022;67:125006.
[68] Mohammadi A, Tashima H, Takyu S, Iwao Y, Akamatsu G, Kang HG, et al. Feasibility of triple gamma ray imaging of 10C for range verification in ion therapy. Phys Med Biol 2022;67:165001.
[69] Parodi K, Assmann W, Belka C, Bortfeldt J, Clevert DA, Dedes G, et al. Towards a novel small animal proton irradiation platform: the SIRMIO project. Acta Oncol 2019;58:1470–1475.
[70] Tashima H, Yamaya T. Compton imaging for medical applications. Radiol Phys Technol 2022;15:187–205.
[71] Safari M, Dedes G, Thirolf P, Zoglauer A, Yamaya T, Durante M, et al., Toward hybrid γ-PET imaging of radioactive ion beams at FAIR, in the Book of Abstracts of the International Biophysics Collaboration Meeting, GSI REPORT 2019-3 https://repository.gsi.de/record/218719/files/ENDVERSIONBioColl_BookOfAbstracts.pdf